Astronomy & Astrophysics manuscript no. virgo˙astroph
March 12, 2014
© ESO 2014

arXiv:1403.2388v1 [astro-ph.GA] 10 Mar 2014

A comprehensive view of the Virgo Stellar Stream

Sonia Duffau[1,2], A. Katherina Vivas[3], Robert Zinn[4], René A. Méndez[5], and María Teresa Ruiz[5]

[1] Zentrum für Astronomie der Universität Heidelberg, Landessternwarte, Königstuhl 12, D-69117, Heidelberg, Germany
e-mail: sduffau@lsw.uni-heidelberg.de
[2] Zentrum für Astronomie der Universität Heidelberg, Astronomisches Rechen-Institut, Mönchhofstraße 12-14, D-69120 Heidelberg, Germany
e-mail: sduffau@ari.uni-heidelberg.de
[3] Cerro Tololo Interamerican Observatory, Casilla 603, La Serena, Chile
e-mail: kvivas@ctio.noao.edu
[4] Department of Astronomy, Yale University, P.O. Box 208101, New Haven, CT 06520-8101, USA
e-mail: robert.zinn@yale.edu
[5] Departmento de Astronomía, Universidad de Chile, Casilla 36-D, Santiago, Chile
e-mail: rmendez@u.uchile.cl, mtruiz@das.uchile.cl

Preprint online version: March 12, 2014

ABSTRACT

To explore the complex halo substructure that has been reported in the direction of the Virgo constellation, radial velocities and metallicities have been measured for 82 RR Lyrae stars (RRLS) that were identified by the QUEST survey. These stars are distributed over 90 sq. deg. of the sky, and lie from 4 to 23 kpc from the Sun. Using an algorithm for finding groups in phase space and modeling the smooth halo component in the region, we identified the 5 most significant RRLS groups, some of which were previously known or suspected. We have examined the SEKBO and the Catalina catalog of RRLS (with available spectroscopic measurements by Prior et al. 2009, and Drake et al. 2013), as well as the bright QUEST RRLS sample (Vivas et al. in prep.), the catalogs of blue horizontal branch (BHB) stars compiled by Sirko et al (2004) and Brown et al (2008, 2010) and the catalog of Red Giant stars from the Spaghetti survey, for stars that may be related to the QUEST RRLS groups. The most significant group of RRLS is the Virgo Stellar Stream (VSS, first reported by Duffau et al 2006) identified here as group A, which is composed of at least 10 RRLS and 3 BHB stars. It has a mean distance of 19.6 kpc and a mean radial velocity $V_{\rm gsr}$ = 128 km s^{-1}, as estimated from its RRLS members. With the revised velocities reported here, there is no longer an offset in velocity between the RRLS in the VSS and the prominent peak in the velocities of main-sequence turnoff stars reported by Newberg et al (2007) in the same direction and at a similar distance (S297+63-20.5). The location in phase space of two other groups (F and H) suggests a possible connection with the VSS, which cannot be discarded at this point, although the turnoff colors of the VSS and group H, as identified from Newberg et al. 2007, suggest they might be composed of different populations. Two more groups, B and D, are found at mean distances of 19.0 and 5.7 kpc, and mean radial velocities of $V_{\rm gsr}$ = −94 and 32 km s^{-1}. The latter is the more numerous in terms of total members, as well as the more extended in RA. A comparison with the latest model of the disruption of the Sagittarius dwarf, indicates that none of the above groups is related to it. Rather than being the result of a single accretion event, the excess of stars observed in Virgo appears to be composed of several halo substructures along the same line of sight.

Key words. Stars: variables: RR Lyrae – Galaxy: abundances – Galaxy: halo – Galaxy: kinematics and dynamics – Galaxy: structure

1. INTRODUCTION

Over the last decade, a number of simulations of galaxy formation that are based on the popular ΛCDM hierarchical picture have predicted that the halos of disk galaxies should contain numerous substructures that are the debris from accreted dwarf galaxies (Bullock & Johnston 2005; Cooper et al. 2010). Over the same period, the evidence that the Milky Way has indeed accreted dwarf galaxies has grown considerably (e.g. Bell et al. 2008; Helmi et al. 2011; Xue et al. 2011). While there is no doubt that accretion has occurred, it is not yet firm that the number and the properties of the observed substructures are consistent with those simulations. To answer this question, it is not only necessary to find the substructures but also to characterize them in sufficient detail that the masses of the dwarf galaxies and the times of their accretion can be estimated. This paper reports a more thorough description of halo substructure in the direction of the constellation Virgo.

After the Sagittarius (Sgr) tidal streams (e.g. Majewski et al. 2003), the Virgo region contains the most obvious overdensity of stars in the sky explored so far by large scale surveys. Discovered as an overdensity of RR Lyrae stars (RRLS) in the QUEST survey (Vivas et al. 2001; Vivas 2002; Vivas & Zinn 2006; Duffau et al. 2006) and of main-sequence turn-off stars (Newberg et al. 2002) in the SDSS, it is one of the most noticeable features in the Field of Streams (Belokurov et al. 2006). Based in main sequence stars from SDSS, Jurić et al. (2008) estimated that the substructure, covers ∼ 1000 sq deg of the sky. More recently, Bonaca et al. (2012) suggested the feature may span up to ∼ 3000 sq deg. Jurić et al. (2008) suggested that the Virgo overdensity (VOD) was produced by the merger of a low surface brightness galaxy with the Milky Way (see also Carlin et al. (2012)). Spectroscopic observations have revealed, however, a complex system of substructures in the kinematic distribution of stars (Duffau et al. 2006; Newberg et al. 2007; Vivas et al. 2008; Starkenburg et al. 2009; Prior et al. 2009; Brink et al. 2010; Casey et al. 2012). Furthermore, it ap-

pears that the strengths of these features depend on the tracer used. For example, the strongest peak in the velocity distribution of RRLS and turnoff stars in the region is found near $V_{\rm gsr} = 120$ km s^{-1} (Duffau et al. 2006; Newberg et al. 2007; Prior et al. 2009), while main sequence and K giants show a peak at $V_{\rm gsr} = -80$ km s^{-1} (Brink et al. 2010; Casey et al. 2012).

In their study of substructures in high resolution simulations of galactic halos from the Aquarius project, Helmi et al. (2011) found that debris from massive progenitors often look like diffuse substructures on the sky. They point out that because of the large-scale structure present in the Universe when galaxies began to form, the accretion of galaxies was not random in direction, but was instead along preferred directions. This infall pattern causes the streams and substructures of different progenitors to overlap. This scenario, rather than a single massive progenitor, may be the explanation for the substructures in Virgo. To complicate the picture, the region of the VOD is not far from the leading tail of the Sgr dSph galaxy. Although the bulk of the Sgr stars lie much farther away, at 50 kpc, it has been suggested that stars which became unbound in previous passages of the galaxy may lie at much closer distances (Martínez-Delgado et al. 2007; Prior et al. 2009; Law & Majewski 2010).

Although the distance to the Virgo overdensity is relatively small, the spatial distribution of stars alone does not provide a clear picture of the complex substructure. The densest part of the RRLS overdensity lies at 19 kpc (Vivas & Zinn 2006), but Jurić et al. (2008) suggested that the VOD covered a range of distances from $\sim$ 5 to 20 kpc. Velocities are key to separate the different accretion events and establish the relationship between them, if any.

In this investigation, we obtained spectroscopy of RRLS present in the QUEST survey in the Virgo region between 4 and 23 kpc, with the goal of filling the gap between the earlier investigations by Duffau et al. (2006) and Vivas et al. (2008) who observed QUEST RRLS in ranges 18-20 kpc and < 12 kpc, respectively. The sample of RRLS presented here, which is a combination of new observations and an updating of previous ones, includes 87% of the QUEST RRLS in an area of almost 90 sq degrees of the sky. The relative errors of the RRLS distances are about 7% (Vivas and Zinn 2006), which is superior to most other halo tracers (e.g., $\sim$ 15% for red giants, Starkenburg 2009) and comparable to that obtained for BHB stars, their nearest rival. The pulsations of RRLS make the determination of their systemic radial velocities more difficult than for other stars, but even using small numbers of observations of modest precision, it is possible to obtain precisions of $\sim 15-20$ km s^{-1} (e.g. Layden 1994, Vivas et al. 2005, Prior et al. 2009). Since the line-of-sight (los) velocity dispersion of the halo is $\sim$ 115 km s^{-1} over the distance range considered here Brown et al. (2010), this precision is adequate for identifying the velocity peaks produced by substructure against the background of random halo stars. The main reason to use RRLS as tracers is that even when they do not represent the most numerous population of a system, they provide precise distances and good velocities to help pin-point the location in the sky where to continue searching for evidence of an accretion event. The few RRLS and BHB stars one might find clustered in a particular place in the sky are thus highly significant. The confusion caused by the use of a more numerous tracer with a larger distance error in regions where several stream candidates are suspected can be clarified by the use of RRLS. The trade off is that the number of stars found will be smaller but their parameters will be very reliable.

This paper is organized as follows: in Section 2 we describe the sample of RRLS observed here and its relationship (in space) with other works carried out in the region. Section 3 explains the observations and processing techniques that we have used. We look for coherent groups in the sample of RRLS in Section 4, and investigate whether or not these groups are also found in surveys using different tracers. Finally, we discuss our results in Section 5.

2. THE SAMPLE OF RR LYRAE STARS

We have merged 3 different spectroscopic data sets: 18 RRLS from Duffau et al. (2006), 29 RRLS from Vivas et al. (2008), and 36 RRLS which are reported here for the first time. In this latest data set most stars come from the QUEST survey (Vivas et al. 2004) but we also took spectra of 3 of the RRLS discovered by Ivezić et al. (2000) (and followed up by Wu et al. 2005), with SDSS data just beyond the northern limit of QUEST. As we explain below, the radial velocity measurements of the sample RRLS that was observed by Duffau et al. (2006) have been revised. We have also updated the radial velocity measurements for some stars in the sample of Vivas et al. (2008), for which additional photometric and spectroscopic data have been obtained. For three of the stars in our sample we were able to obtain only their mean metallicities, not their radial velocities.

Most of our targets come from the photometric study performed by Vivas and collaborators on two bands of QUEST data. Each band is a 2.2°-wide stripe at a fixed declination observed multiple times in driftscan mode with the QUEST camera (Baltay et al. 2002), with the 1m Schmidt telescope at the Venezuelan National Observatory of Llano del Hato. The results of the survey in the band centered at Dec = −1° are reported in Vivas et al. (2004); the second band, at Dec = −3°, has not been published yet. The selected QUEST RRLS lie at 178° < RA < 200° and −4.25° < Dec < 0°, while the 3 SDSS RRLS have the same range of RA but 0° < Dec < 1.23°. The RRLS have mean V magnitudes between 13.5 and 17.5 mags, which correspond to a distance from the Sun between 4 and 23 kpc. Figure 1 is a polar plot in which right ascension (RA) and distance from the Sun (d) for our sample are shown in the angular and radial direction, respectively.

To compare our sample with previous ones, we show in Figures 2 and 3 the photometric and spectroscopic detections of substructures in the region. In both figures, the center of the densest part of the overdensity, as seen by the QUEST survey, at (RA, Dec) =(187°,−1°), is shown with a × symbol. Among the detections of substructures in photometric data, there are overdensities of RRLS from the QUEST (Vivas & Zinn 2006, V06) and SEKBO surveys (groups K-A and K-B in Figure 2, Keller et al. 2008), F turnoff stars (Newberg et al. 2002, N02), main sequence stars in SDSS (Jurić et al. 2008, J08), and subgiant stars in SDSS (Keller 2010, K10). In addition, overdensities have appeared in the region by analyzing the luminosity function (Duffau et al. 2006) and by combining main sequence and red giant stars from the SEKBO survey (Keller et al. 2009, K09). A strong main sequence located at $\sim$ 23 kpc was detected by Jerjen et al. (2013) in the three fields shown in Figure 2. One of those fields is coincident with the location of an alleged faint satellite galaxy, Vir Z, discovered by Walsh et al. (2009). However, the results presented by Jerjen et al. (2013) suggest that this object is more extended and it is located much closer than initially thought. Except for the SEKBO survey, which goes along the ecliptic, all other detections come from QUEST and SDSS, which have a southern limit at about Dec = −4° in this part of the sky (shown as a horizontal dotted line in Figures 2 and 3). Three SDSS/SEGUE stripes cross the region toward

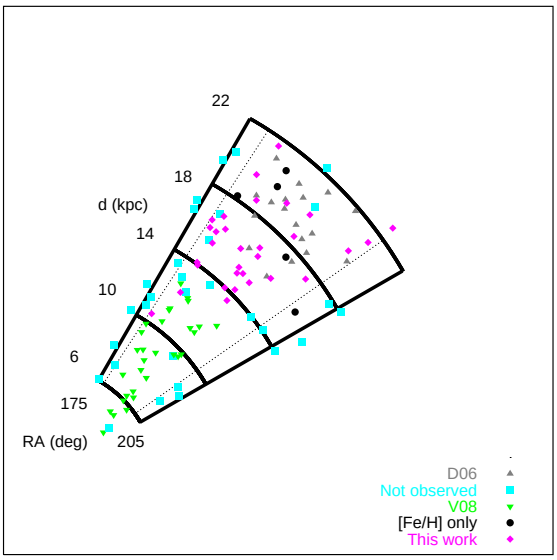

Fig. 1. Distribution of the QUEST RRLS in the sky. The radial direction shows distance from the Sun (d), while the angular direction corresponds to right ascension (RA). Different symbols show the 3 data sets we are using in this work. It can be seen that the new observations (diamond symbols) fill the gap in distance between the samples of Duffau et al. (2006, D06) and Vivas et al. (2008, V08). The square and circle symbols indicate those RRLS for which we did not obtain spectroscopic observations or we were not able to measure a radial velocity. We concentrate our analysis in the region between the two dotted radial lines ($178^\circ < \mathrm{RA} < 200^\circ$), in which we have phase space information for most of the QUEST RRLS.

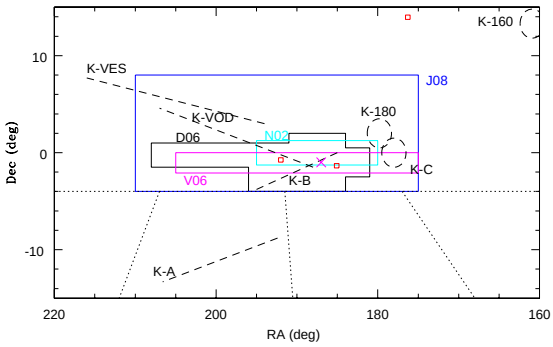

Fig. 2. Distribution in the sky of the different photometric detections of sub-structures in the Virgo region. The dotted horizontal line at Dec = −4° represents the rough southern limit of the SDSS imaging survey. There are also 3 SEGUE imaging stripes that cross the region at negative declinations as shown by the other dotted lines. Labels correspond to the following references: N02, Newberg et al. (2002); V06, Vivas & Zinn (2006); D06, Duffau et al. (2006); J08, Jurić et al. (2008); K-A, K-B and K-C, Keller et al. (2008, 2009); K-VOD, K-VES, K-160 and K-180, Keller (2010). The small squares represent the fields observed by Jerjen et al. (2013); the one at (RA, Dec) = (185°, −1.°4) coincides with the location of Vir Z (Walsh et al. 2009). The × symbol shows the densest part of the overdensity as seen in RRLS in the QUEST survey.

southern declinations (also shown as dotted lines). From these stripes and the SEKBO survey, it has been suggested that the VOD extends to the south, beyond the SDSS and QUEST limits (Newberg et al. 2007; Keller et al. 2008; Prior et al. 2009).

Detections of substructure by radial velocity have been made through the measurement of either many stars in relatively small fields, (Newberg et al. 2007; Brink et al. 2010; Casey et al. 2012), or relatively few stars but widely distributed over the region (Duffau et al. 2006; Vivas et al. 2008; Prior et al. 2009; Starkenburg et al. 2009). The latter usually involves targets for which good distance determination is possible. Hence, precise positioning of any stream in the sky is guaranteed, at the expense of a low number of members. Following this idea, Duffau et al. (2006) measured RRLS in the densest part of the overdensity (as seen by QUEST) at 19 kpc, and found a coherent velocity at $V_{\rm gsr} \approx 100$ km s^{-1} (but see revision below), which was dubbed the *Virgo Stellar Stream* (VSS). Also, the SEKBO survey of RRLS (P09 Prior et al. 2009), and red giants from the Spaghetti survey (S09 Starkenburg et al. 2009) found several groups of stars with similar distance and radial velocity. Those groups are shown as circles and triangles connected by lines in Figure 3.

Casetti-Dinescu et al. (2009) measured the proper motion of one of the QUEST RRLS within the region of the overdensity, which has a radial velocity consistent with being a member of the VSS. The measured star and the direction of the proper motion is shown with a star symbol and an arrow in Figure 3. The path of a tentative past orbit calculated by the authors is shown with a dot-dashed lined. This orbit has been confirmed recently by Carlin et al. (2012) using proper motions for a more extended sample of turnoff stars.

3. OBSERVATIONS

3.1. Telescopes and setups

A total of 179 spectra of 82 RRLS (covering about 90 sq degrees in the sky), have been analyzed, including revisions of previous measurements. The fainter stars were observed with the Magellan, WIYN, Blanco, and ESO 3.6m telescopes, while we used the 1.5m telescopes at both La Silla and CTIO (SMARTS) for the brighter ones. Table 1 displays the details of all the telescopes and instrument setups used in this work. Most of the SMARTS observations were obtained in service mode.

Most of the spectra were taken in the blue part of the optical window, allowing the measurement of Balmer lines (excluding Hα) and the Ca II H and K lines. However, with the WIYN telescope we used also a "red" and a "green" configuration; this was done mainly to fit some of our targets within other scientific programs at this telescope. In Figure 4 we show the spectra of stars #208, #728 and #227 which represent spectra in the three different wavelength ranges covered by our telescope/setup combinations. Some characteristic spectral lines of RRLS are marked for reference. Only the blue spectra were used for measuring metallicities, which require a measurement of the CaII K line. Typical spectra for this project had a signal to noise of 20 or larger, which is at the same time the minimum we used for estimating metallicities. Radial velocities could be estimated, if necessary, from spectra with a slightly lower signal to noise, but this happened in only a few cases since the quality of the majority of the spectra was high.

Table 1. Telescopes and Instruments

Observatory	Telescope	Instrument	Code	Grating (mm^{-1})	Spectral range (Å)	Resolution (Å)	Dates
La Silla	1.5m	B&C	ESO1.5m	600	3300-5500	3.1	June 2001
La Silla	3.6m	EFOSC2	ESO3.6m	600	3270-5240	5.4	Jan-Feb 2006
LCO	Clay	B&C	Mag05	600	3110-6130	4.3	March 2005
LCO	Clay	LDSS3	Mag07	1090	3440-6140	2.1	February 2007
CTIO	4m	RC-BAS	4m	316	3480-6460	5.7	Jan, Mar 2006
CTIO	1.5m	R-C	SMARTS	600	3532-5300	4.3	2003-2004, 2006-2008
KPNO	WIYN	Hydra	WIYN-B	400	3500-6200	7.1	Apr 2006,Feb 2007,Feb 2008
KPNO	WIYN	Hydra	WIYN-R	600	7100-10000	2.9	Mar 2003,Apr 2007,May 2007
KPNO	WIYN	Hydra	WIYN-G	600	4000-6800	4.6	May 2008

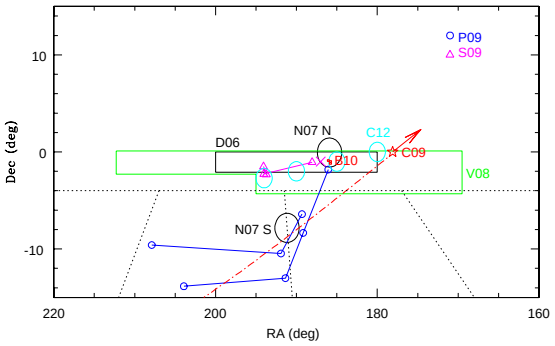

Fig. 3. Similar to Figure 2 but for kinematic detections. The dotted lines and the × symbol are the same as in Figure 2. Labels correspond to the following references: D06 (internal rectangle), Duffau et al. (2006), N07 N and N07 S (large circles), Newberg et al. (2007); V08 (polygon), Vivas et al. (2008); S09 (small triangles), Starkenburg et al. (2009); P09 (small circles), Prior et al. (2009); B10 (tiny squares), Brink et al. (2010); C12 (medium size circles), Casey et al. (2012). The star symbol, arrow and dot-dashed line correspond to the location of an RRLS whose proper motion was determined by Casetti-Dinescu et al. (2009) (C09), the direction of the proper motion and part of the past orbit, respectively.

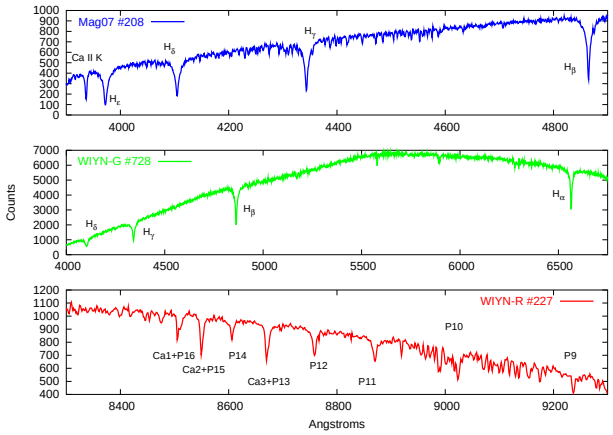

Fig. 4. Example of reduced spectra of RRLS taken with some of the telescopes/setup combinations used for this project. The panels display the three wavelength ranges in use and identify typical spectral features in each of them. The telescope/setup labelling in each panel follows the code defined in Table 1.

3.2. Observing and Reduction Techniques

Since RRLS are pulsating stars, the radial velocity changes during the pulsation cycle. In order to determine the systemic velocity of the star, a curve must be fitted to the radial velocity measurements. We tried to obtain at least two spectra per star, taken at different phases during the cycle, but this was not always possible. As many as 4 spectra were obtained for a few stars.

Since the radial velocity curve of a type ab RRLS has a large discontinuity during the rising branch phase, we avoided taking spectra at phases > 0.85 and < 0.1. Because most observations were made in visitor mode, we were able to control the exact phase at which each star was observed using the ephemerides from the QUEST survey. Not only did we avoid the rising branch but we also spaced in phase the observations for the same star for a better fitting of the radial velocity curve. In service mode, all the spectra were taken at random phases. Some of them were not usable because they were obtained on the rising branch, but since this is a rapid phase, only few observations were lost. We did not control the phase of observation in the WIYN/Hydra observations either, because several RRLS in a Hydra field were observed at the same time.

When possible, we took comparison lamp exposures before and after each program star, to account for any flexure of the instrument. In few cases, spectra were reduced using only one of the lamps; in all others, the average of the wavelength calibrations obtained with both lamps was used to calibrate our spectra. The data were reduced using standard IRAF[1] tasks or packages specifically made for an instrument. Wavelength calibration was performed manually and carefully for each spectrum. The wavelength calibrations had a typical RMS of ~ 2 km s^{-1}.

3.3. New Photometry, New Ephemerides

Following the methodology of Vivas et al. (2008), we improved the ephemerides of the QUEST RRLS by adding new photometric data for many of our stars and by fitting an RRLS template to the light curves. The new photometric observations came mainly from QUEST scans taken after the publication of the first catalog. A few additional observations were obtained with the 0.9 SMARTS telescope at CTIO. The fitting of the light curve used χ^2 minimization with either templates produced by Layden (1998) for type ab stars, or our own template for type c ones (Vivas et al. 2008). We used the original light curve parameters

[1] IRAF is distributed by the National Optical Astronomy Observatory, which is operated by the Association of Universities for Research in Astronomy (AURA) under cooperative agreement with the National Science Foundation.

(namely, period, amplitude, phase at maximum light and maximum magnitude) as initial values and allowed them to vary. The new observations of a few of the type c variables showed that their published periods were spurious. The new light curve parameters are part of the table with the final results of this paper (§ 4). The new photometry for these stars will be included in an upcoming paper.

For most stars the changes in the light curve parameters were minimal. But even a small change in the date at maximum light may have an effect on the calculation of the phase of a spectrum. There were a few stars (#174, 180, 201, 203 and 217) for which the changes were more significant. These stars are included in the new La Silla-QUEST survey (Zinn et al. (2014)). Although these low amplitude variables were originally classified as type c RRLS in the QUEST catalog Vivas et al. (2004), the light curves of La Silla-QUEST, which have a much larger number of epochs (~80 to 190), have long periods and clear signs of asymmetry. The shorter periods assigned by QUEST are aliases of the true ones. These stars were then re-classified as type b and we used the La Silla-QUEST light curve parameters in further calculations.

With these new improved ephemerides we re-calculated the phases at which our old spectra from Duffau et al. (2006) and Vivas et al. (2008) were observed. Consequently, the final radial velocities for these data sets have changed and are updated here.

The La Silla-QUEST data also helped to identify star #241 (reported as a type c in Vivas et al. 2004, 2008) as a WUMa eclipsing binary. If the light curve is phased with twice the period reported in our previous work, it is easy to recognize that the two minima have different depths, a clear sign of eclipsing systems. We therefore eliminated #241 from further analysis.

3.4. Radial Velocities and Metallicities

Except for the case of the red setup for WIYN data, the radial velocities of the target stars were measured with the IRAF task *FXCOR*. *FXCOR* performs fourier cross-correlation between a program star and a radial velocity standard star. In the case of the redder WIYN data, we calculated the velocities in a different way, by measuring the centers of some spectral lines. In both cases we followed very closely the methods explained in Vivas et al. (2008), which will not be repeated here. We discuss only relevant changes in the strategy applied specially to the data of the largest telescopes (Magellan and the 3.6m telescope).

The cross-correlation technique requires selecting radial velocity standards of similar spectral types as the target to be observed during the corresponding run. For all the runs, we observed several of the radial velocity standard stars from Layden (1994) (from now on simply Layden standards). They are listed in Table 2. Velocities in this table are updated values taken from the SIMBAD database. Not all the standards in Table 2 were observed in every run, but we observed several each night. Some standards were observed several times during the same night or in different nights within the same observing run. The Layden standards have the advantage of serving as metallicity standards as well. We used these standards for cross-correlating all SMARTS and ESO 1.5m observations. However, they are bright stars which are hard to observe at large telescopes. During the progress of this work we found the need to set up different standard stars. One set came out of a group of Blue Metal Poor stars studied by Preston & Sneden (2000) (from now on, Preston-Sneden standards). These standards were observed only in the Mag07 run. The Preston-Sneden standards are closer in magnitude to our target stars. We selected four non variable stars from Preston & Sneden (2000) which were available in the sky at the time of the observing run. From Preston & Sneden (2000), these stars have small dispersions in their radial velocities, from 0.52 km s^{-1} to 0.73 km s^{-1}.

Finally, we created another set of standards by degrading high resolution spectra obtained from the ELODIE archive (Moultaka et al. 2004) to the resolution of our spectra. We did this for each of the telescope-instrument setups. We refer to this set as the ELODIE standards. These stars have velocity estimates[2] better than 0.1 km s^{-1}. Tables 3 and 4 contain all of the relevant information of the radial velocity standard stars used in these two sets.

For the ELODIE standard set we selected 13 stars with spectral types F, which are similar to the ones of RRLS. To degrade the ELODIE spectra to the proper resolution we used the IRAF tasks *gauss*. These degraded spectra were then binned to match the binning of the targets using *dispcor*. Finally, we normalized the spectra by using *continuum*, and trimmed the large spectral range of the ELODIE spectra to match that of the target spectra.

Errors were estimated for each set of standard stars and instrumental setup by cross correlating every standard with all others, and getting the difference between the velocity obtained for each star and its velocity from the literature. This procedure revealed that some of our observations of Layden standard stars were off. Centering these bright stars incorrectly on the slit may have produced a significant shift in the spectrum.

For the Mag07 run we used the Preston-Sneden standards for cross-correlation, and we used the ELODIE standards for the 3.6m telescope observations. We then decided to revise the measurements of the stars from the Mag05 run, which were reported in Duffau et al. (2006). The use of ELODIE standards on these observations produced significantly better results, and the new measurements agree with the results obtained by Newberg et al. (2007) for F turnoff stars in the region (see § 4.1).

The estimated error for the radial velocities (σ_r) of the Mag07 run is 13 km s^{-1}, while for the 3.6m telescope is 9 km s^{-1}. The estimated errors from the SMARTS, WIYN (blue, green and red setups) and ESO 1.5m telescope data sets are, 16, 8, 6, 9 and 12 km s^{-1}, respectively.

Unfortunately, the data from the 4m Blanco telescope at CTIO proved to be unsuitable for radial velocity measurements, as shifts of one pixel or more were found in the raw data on consecutive exposures of the same star. Nevertheless, we could measure the metal abundances of these stars because the typical shifts (of about 1 pixel), represent ~ 1 Å, which is very small compared the width of the spectral features used in Layden's method of determining [Fe/H]. Using this method, which is only applicable to the blue spectra, we measured [Fe/H] with precisions of 0.15 and 0.2 dex for types ab and c, respectively. See our previous investigations for more details (Vivas et al. 2005; Duffau et al. 2006; Vivas et al. 2008).

Although the dependence of the absolute magnitude of RRLS ($M_V(RR)$) on metallicity is small, we took advantage of the fact that we had spectroscopic measurements for almost all stars in our sample. We calculated the distances to the stars using the relationship in Demarque et al. (2000):

$$M_V(RR) = 0.22[\mathrm{Fe/H}] + 0.90 \quad (1)$$

For the few stars for which we did not measure a metallicity, we assumed $M_V(RR) = +0.55$, which corresponds to a metallicity of [Fe/H]= −1.6 in the above equation.

[2] private communication, Sergio Ilovaisky (Observatoire de Haute-Provence).

Table 2. Selected Layden stars for use as radial velocity and metallicity standards

Star	Radial Velocity (km s^{-1})	V
Feige 56	34.6	11.1
Kopff 27	5.5	10.2
HD 693	17.0	4.9
HD 22413	34.8	8.7
HD 65925	-8.2	5.2
HD 74000	205.6	9.4
HD 74438	20.4	7.9
HD 76483	5.4	4.9
HD 78791	22.4	4.5
HD 140283	-171.4	7.3
HD 154417	-18.0	5.8

Table 3. Selected Preston-Sneden stars for use as radial velocity standards

Star	RA	Dec	V	(B-V)	[Fe/H]	Radial Velocity
	(J2000)	(J2000)				(km s^{-1})
22175-034	02 20 21.4	-10 38 10	12.6	0.34	-0.28	27.2
22185-009	03 14 53.8	-14 43 46	13.8	0.30	-1.67	-100.6
22874-009	14 34 23.0	-26 17 39	13.7	0.24	-0.42	-36.7
22874-042	14 38 01.7	-24 58 47	14.0	0.33	-1.53	176.2

Table 4. Selected ELODIE stars for use as radial velocity standards

Star	RA	Dec	B	V	Spectral Type	Radial Velocity
	(J2000)	(J2000)				(km s^{-1})
HD 102870	11 50 41.7185	+01 45 52.985	4.16	3.61	F9V	4.43
HD 13555	02 12 48.0855	+21 12 39.575	5.64	5.24	F5V	5.55
HD 136202	15 19 18.7977	+01 45 55.468	5.60	5.10	F8III-IV	54.41
HD 140283	15 43 03.0966	-10 56 00.590	7.69	7.24	sdF3	-169.83
HD 16895	02 44 11.9863	+49 13 42.412	4.60	4.12	F7V	24.44
HD 19994	03 12 46.4365	-01 11 45.964	5.63	5.06	F8V	19.21
HD 222368	23 39 57.0409	+05 37 34.650	4.64	4.13	F7V	5.62
HD 22484	03 36 52.3832	+00 24 05.982	4.86	4.28	F9IV-V	28.08
HD 22879	03 40 22.0645	-03 13 01.133	7.23	6.74	F9V	120.19
HD 3268	00 35 54.8015	+13 12 25.442	6.93	6.41	F7V	-23.40
HD 49933	06 50 49.8319	-00 32 27.175	6.14	5.78	F2V	-12.57
HD 693	00 11 15.8573	-15 28 04.719	5.38	4.89	F8Vfe-08H-05	15.04
HD 7476	01 14 49.1720	-00 58 25.661	6.12	5.70	F5V	25.49

4. Results

Table 5 contains all the individual observations of the RRLS investigated here. Many stars have multiple entries in this table since they were observed more than once at different epochs. The table includes the revised velocities of the stars first reported in Duffau et al. (2006). The phase at which the spectra in Duffau et al. (2006) and Vivas et al. (2008) were taken has been recalculated in this table using the new ephemerides.

Figure 5 shows examples of the radial velocity curves fitted to three different stars. The complete sample of radial velocity curves for stars having 2 or more observations are available in the online version of this article. As can be seen in Figure 5 (and its online companions), there is good consistency among the results from different instrumental setups, which give us confidence that there are no significant systematic differences among the data sets. Within errors, there is also consistency in the metallicities determined for the same star from data coming from different telescopes. Table 6 contains the final results for all the 82 stars in the sample, after fitting the radial velocity curves and averaging metallicities obtained from the individual spectra. Because of the revision on velocities and ephemerides, this table supersedes the one in Vivas et al. (2008). Table 6 contains: ID, RA, Dec, mean extinction-corrected magnitude (V_0), period in days, heliocentric Julian day at maximum light (HJD_0), type of RRLS, distance from the Sun in kpc (d), number of spectra used for the radial velocity curve fitting (Nfit), heliocentric radial velocity (V_γ), rms of the fitting of the radial velocity curve (σ_{fit}), final error in the systemic velocity (σ_γ), radial velocity in the galactic standard of rest (V_{gsr}), and metallicity [Fe/H]. For details on how the final error in the systemic velocities were calculated we refer the reader to Vivas et al. (2008).

4.1. Revision of Duffau et al. (2006)

From the analysis of our first spectroscopic data (18 RRLS and 10 BHB stars from Sirko et al. (2004)), we concluded in Duffau et al. (2006) that there was kinematical evidence for a stellar stream (the VSS) at $\sim$ 19 kpc from the Sun. These first results indicated that a velocity peak at $V_{gsr} \sim 100$ km s^{-1} with a dispersion of $\sigma \sim 17$ km s^{-1}, and a mean metal abundance estimated in [Fe/H] = -1.86 and $\sigma = 0.40$ existed within the clump of RRLS. The BHB stars in that work were taken from SDSS

Table 5. Individual observations of the target RR Lyrae stars

Star	HJD	Exp	Telescope	Phase	V_r	σ_r	[Fe/H]
	(+2450000 d)	(s)			(km s^{-1})	(km s^{-1})	
172	3737.8304	520	ESO3.6m	0.270	-25	11	-1.75
175	3831.6760	1200	WIYN-B	0.208	180	15	-2.19
175	4153.8770	3600	WIYN-B	0.572	292	8	-2.36
176	3737.8091	400	ESO3.6m	0.538	396	15	-1.41
176	4153.8770	3600	WIYN-B	0.023	366	8	...
177	3436.6576	800	Mag05	0.565	266	17	-2.26

Notes. This table is available in its entirety in the only version of this article. A portion is shown here for guidance regarding its form and content. The table displays the ID of the star, following the QUEST catalog, the heliocentric julian date for the observation, the exposure time in seconds, the telescope/setup used, the estimates for phase, radial velocity, radial velocity error, and metallicity. The telescope/setup column corresponds to the codes defined in Table 1.

Table 6. RR Lyrae data: positions, light curve parameters, systemic velocities and metallicity

ID	RA	Dec	V_0	Period	HJD_0	Type	d	Nfit	V_γ	σ_{fit}	σ_γ	V_{gsr}	[Fe/H]
	(deg)	(deg)		(d)	(+2450000 d)		(kpc)		(km s^{-1})	(km s^{-1})	(km s^{-1})	(km s^{-1})	
172	180.185025	-0.712449	16.54	0.52119	1610.71317	ab	16.0	1	2	0	17	-104	-1.75
175	180.632505	-1.895691	16.14	0.57091	1582.74254	ab	14.1	2	249	34	34	140	-2.28
176	181.087335	-2.178318	16.38	0.33061	1971.84326	c	14.4	2	385	4	7	276	-1.41
177	181.212600	-0.351735	17.03	0.37668	1585.81581	c	21.0	2	261	3	13	158	-2.19
182	182.130810	-0.788163	16.80	0.59315	1620.71096	ab	18.8	1	-25	0	22	-128	-2.16

Notes. This table is available in its entirety in the online version of this article. A portion is shown here for guidance regarding its form and content. See text for description.

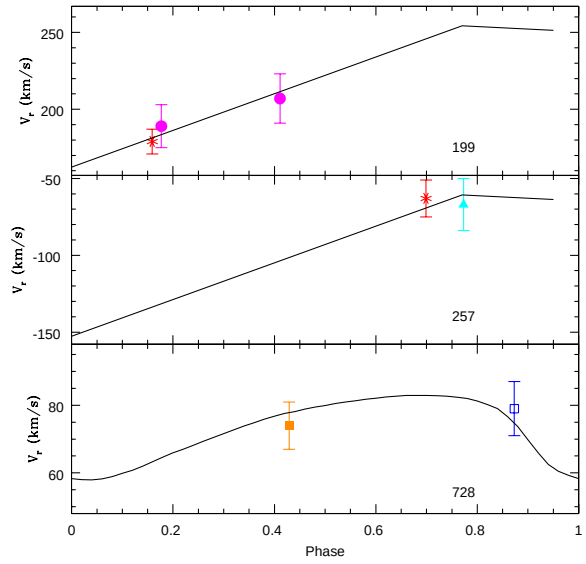

Fig. 5. Example of radial velocity curves fitted to the data of stars 199, 257 and 728. The first two are RRab while the last one (bottom panel) is a type c star. These stars were observed with different telescopes. The consistency of the data is reassuring that no large systematic offsets are present in the data. Solid circles represent velocities measured in Magellan runs; asterisks, open square and solid square correspond to different WIYN setups (red, blue and green, respectively); triangle is a measurement from the ESO 3.6m telescope. The complete set of radial velocity figures are available as online only material.

DR1, as selected by Sirko et al. (2004). We use below the updated velocities of these BHB stars from SDSS DR7.

Figure 6 displays the new velocity histograms for the densest region of the overdensity (at $\sim$ 19 kpc), as defined in Duffau et al. (2006). There are 9 stars (8 RRLS and 1 BHB star) in this region. In the revised histogram shown in Figure 6, which can be directly compared with Fig. 2 (top) in Duffau et al. (2006), there is a clear peak in the velocity distribution, which contains the same 6 stars as in the previous paper, but the peak is slightly shifted toward more positive velocities. The new mean of this kinematical group is V_{gsr} = 128 km s^{-1} and it has a standard deviation of σ = 19 km s^{-1}. The mean velocity is now even further away from the model halo without rotation, (0 km s^{-1}), and the standard deviation is still only slightly higher than our mean observational error. More importantly, the new mean velocity now agrees very well with the result of V_{gsr} = 130 km s^{-1} that Newberg et al. (2007) found in the S297+63-20.5 feature from spectroscopy of turnoff F stars. Although S297+63-20.5 and the VSS are virtually in the same part of the sky (see Figure 2) and at the same distance, Newberg et al. (2007) were reluctant to associate both features because of the offset in velocity. The revision of our velocities, removes the offset to within observational errors. Thus, the VSS and S297+63-20.5 refer to the same halo substructure.

4.2. Radial Velocity Distribution in the Virgo Region

Figure 7 shows the distribution of radial velocities for all the stars in the sample. We proceed to examine the velocity histogram for deviations with respect to the expected smooth non-rotating halo model. The mean radial velocity is 31 km s^{-1} with a standard deviation of 124 km s^{-1}. The expected distribution of halo field stars at the mean distance of the sample of these RRLS, $\sim$ 15 kpc, has a standard deviation of $\sim$ 116 km s^{-1}, according to the velocity profile measured by Brown et al. (2010), and it is shown by the dashed Gaussian line in Figure 7. From this figure it is clear that there are important deviations of our data with respect to the expected normal distribution, which suggest that substructures may be present. Because we have taken the complete sample of stars to make this histogram, the information

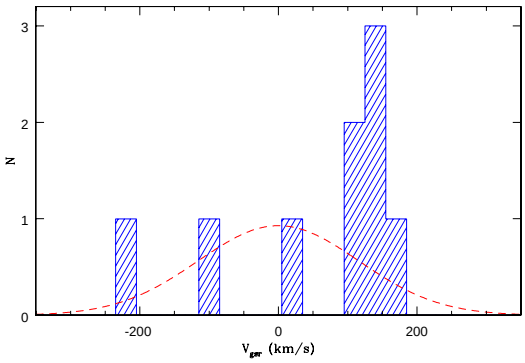

Fig. 6. Radial velocity distribution of 9 RRLS and 1 BHB star in the densest part of the VSS region. For reference, the expected distribution of the same number of halo stars at the distance of this region is shown as a Gaussian curve ($\langle V_{\rm gsr}\rangle$ = 0 km s^{-1}, σ = 116 km s^{-1}).

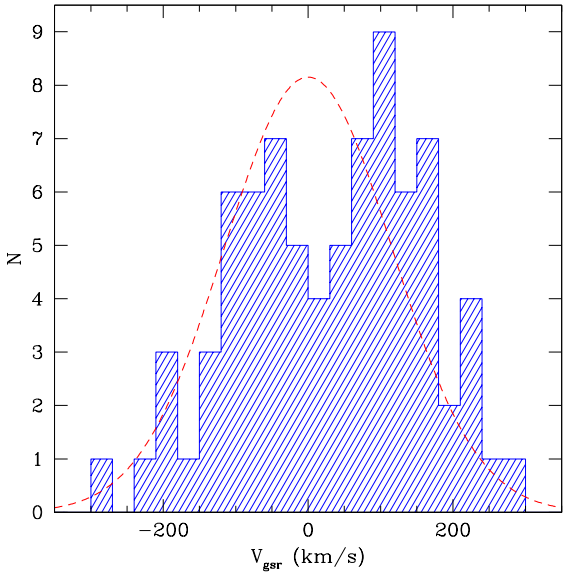

Fig. 7. Radial velocity distribution of 79 RRLS in the Virgo region. Bin size is 30 km s^{-1}. For comparison, the expected distribution of the same number of halo stars at the average distance of these RRLS is shown as a Gaussian curve ($\langle V_{\rm gsr}\rangle$ = 0 km s^{-1}, σ = 116 km s^{-1}).

about the distribution in distance of the velocity deviations is not evident.

A better sense of where the kinematic groups may be located can be seen by splitting the velocity histogram into four distance bins (Figure 8). We examined each bin separately, and found evidence of velocity groups in two of them.

18-23 kpc bin: The most distant bin (top panel in Figure 8) shows the distribution of the 23 RRLS with $d > 18$ kpc. The distribution of velocities is definitely non-Gaussian and this is confirmed by a Shapiro-Wilk test which rejects normality at the 97% confidence level. This panel corresponds to the range of distances where the VSS was first detected by Duffau et al. (2006). The VSS is seen in this histogram as 7 stars with $120 \lessapprox V_{\rm gsr} \lessapprox 180$ km s^{-1}. But, with the inclusion of more stars to the original

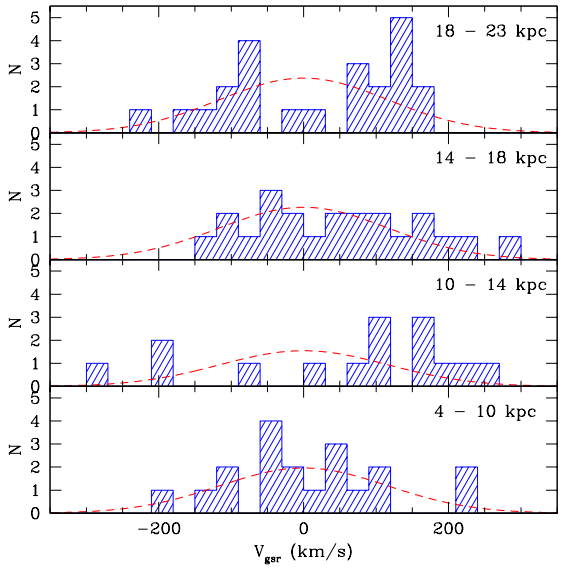

Fig. 8. Radial velocity distribution of our stars in 4 different distance bins. Gaussian curves representing a halo smooth distribution are shown for the same number of stars contained in each distance bin.

Duffau et al.'s sample, a second peak in the distribution is now easily observed at $V_{\rm gsr} \sim -75$ km s^{-1}.

10-14 kpc bin: The distribution of velocities in the range of distances $10 < d < 14$ kpc also shows hints of substructures since an excess of stars at very high positive velocity (> 150 km s^{-1}) is present. This peak is mostly made out of the stars already reported in Vivas et al. (2008). A second peak is seen at $V_{\rm gsr}$ = 105 km s^{-1}. In this distance bin, normality in the velocity distribution is also rejected by the Shapiro-Wilk test at the 95% confidence level. The stars in this bin have a mean velocity $\langle V_{\rm gsr}\rangle$ = 57 km s^{-1}, which is significantly offset from the nominal value of the halo; this is of course due to the presence of the two positive velocity groups. The standard deviation is also significantly larger than the nominal halo, σ = 166 km s^{-1}.

bins 4-10 kpc and 14-18 kpc: These two bins do not show significant features in the velocity distribution. According to Shapiro-Wilk statistical test there is no reason to suspect the stars in these bins are not drawn from a normal distribution.

Since we chose arbitrarily the limits of the distance bins in the four panels of Figure 8, it is possible that the identified velocity groups extend beyond the limits where they are recognized. In the following sections, we will apply a group finding algorithm to the RRLS without imposing distance bins.

4.3. Group Finding Algorithm

To find groups of stars in phase space we have used the idea of *Stellar Pairs*, inspired by the works of Clewley & Kinman (2006); Vivas et al. (2008) and Starkenburg et al. (2009). Two stars make a stellar pair when they are close in space and their velocities are similar. A group is formed when two or more pairs have stars in common. Thus, the minimum number of members in a group is 3 (two pairs with 1 star in common).

Starkenburg et al. (2009) define a "pair" of stars based on the *four-distance*, $4d_{ij}$, between stars i and j:

$$(4d_{ij})^2 = \omega_\phi^2 \phi_{ij}^2 + \omega_d (d_i - d_j)^2 + \omega_v (v_i - v_j)^2 \qquad (2)$$

where the first term on the right hand of the equation represents the angular distance of two stars in the sky, and the second and third terms are their differences in distance from the Sun and radial velocity, respectively. Each term is weighted by the values ω_ϕ, ω_d and ω_v, defined in Starkenburg et al. (2009), to take into account the observational errors and to normalize to the maximum possible separation between the two stars. With this definition, two stars make a pair when $4d_{ij} < \epsilon$, where ϵ is a free parameter that gives a measurement of how tight the groups are in phase space.

A potential problem with the above formalization is that the maximum allowed separation in the sky (measured in degrees) means different physical scales of the projected size in kpc of a group of stars in the sky, depending on their distance from the Sun. This means that with increasing distance, the method imposes the search of groups which are tighter in the direction perpendicular to the line of sight compared with the allowed size along the line of sight. This is not appropriate for the search of cold streams, where the constraint in distance separation must remain the same along the stream independent of orientation or distance from the Sun.

Here we propose a modification on the definition of the four-distance to ensure that at any place in the Galactic halo, the method does not impose any preference to the physical scale along one dimension or the other:

$$(4d_{ij})^2 = \omega^2_{3d_{ij}}(3d_{ij})^2 + \omega_v(v_i - v_j)^2 \quad (3)$$

where $3d_{ij}$ is the three-dimensional distance between two stars calculated from their galactocentric cartesian coordinates (x,y,z):

$$3d_{ij} = \sqrt{(x_i - x_j)^2 + (y_i - y_j)^2 + (z_i - z_j)^2} \quad (4)$$

The weights in equation 3, $\omega_{3d_{ij}}$ and ω_v, are defined following Starkenburg et al. (2009) as:

$$\omega_{3d_{ij}} = \left(\frac{1}{(3d)_{max}}\right)^2 \frac{\left(\frac{\sigma d_i}{d_i}\right)^2 + \left(\frac{\sigma d_j}{d_j}\right)^2}{2\langle\frac{\sigma d}{d}\rangle^2} \quad (5)$$

$$\omega_v = \left(\frac{1}{v_{max}}\right)^2 \frac{\sigma v_i^2 + \sigma v_j^2}{2\langle\sigma v\rangle^2} \quad (6)$$

The weights are normalized by the maximum possible range in distance and velocity for two stars which we set to $(3d)_{max}$ = 60 kpc and v_{max} = 550 km s^{-1}. With a σ of 116 km s^{-1} (Brown et al. 2010) for the distribution of the radial velocities of halo stars, the value of v_{max} encloses 2.2σ of the distribution. On the other hand, the number of RRLS farther away than 60 kpc from the galactic center is very low (Sesar et al. 2007; Zinn et al. 2014) and thus it is an appropriate value for $(3d)_{max}$. For the weight in the (3d) distance we only took into account the error in distance along the line of sight since the errors in position of the stars (less than 1″) are negligible compared with the typical separation between stars in a pair (a few degrees).

The critical value ϵ establishes how small is the separation of two stars in space and in velocity. It is a measure of the scale of clumpiness of the groups. The smaller the values of ϵ, the tighter the groups of stars. Table 7 shows the maximum values in 3d distance and velocity for stars in a pair for different values of ϵ, which are obtained by making two stars having one of the parameters (either 3d distance or velocity) exactly the same. In practice stars in a pair will have separations smaller than the values quoted in the table since it is unlikely to have two stars with exactly the same position or velocity. Small values of ϵ may impose constraints which are too tight for the expected density of stars in a stream, velocity dispersion of a typical stream, and for the observational errors of our sample. For example, the maximum separation in velocity of a pair of stars with ϵ = 0.02 is only 10 km s^{-1}, which is smaller than our observational errors. On the other hand, very large values of ϵ may be unable to distinguish individual groups, since they will pair the whole sample into one big group.

Table 7. Maximum values for stars in a pair

ϵ	3d (kpc)	v (km s^{-1})
0.02	1.2	10
0.03	1.8	15
0.04	2.4	20
0.05	3.0	25
0.06	3.6	30

For our RRLS sample we explored different values of ϵ in the range from 0.02 to 0.07 and we found pairs and groups with all of them. We show in Figure 9 some examples of the groups we found with three different values of ϵ (0.04, 0.046 and 0.06). The plots show the distribution in phase space of each one of the groups that were detected with a different color/symbol. The same group may be detected with different values of ϵ. A tight group (small ϵ) may get more members with increasing ϵ (for example, the solid green squares at $\sim$ 130 km s^{-1}), unless it is physically a very concentrated and isolated clump in phase space (for example, the solid cyan stars at $\sim$ 40 km s^{-1}). Other groups just appeared for the first time with the largest value of ϵ. In the figure it can be seen that both the number of groups and the number of members in each group increase with ϵ, until ϵ = 0.06 where the number of groups starts to decline. This is a sign that the maximum allowed separations in distance and velocity are too large and several groups have merged together. In addition, for $\epsilon \geq 0.05$ we obtained several groups that have velocity dispersions larger than the expectations for cold substructures in the halo (which should be below $\sim$ 30 km s^{-1}). Some groups also have an unusually large range in distance along the line of sight, covering in some cases almost the whole range of the RRLS sample. Examples of this can be seen in the lower panel of Figure 9 which shows the results for ϵ = 0.06. Some of the groups (for example, the red open circles at ~ -75 km s^{-1}) are just too dispersed both in distance and velocity to believe they are part of a real cold substructure. Thus, the optimal value of ϵ for finding cold substructures in the RRLS samples seems to be a value below 0.05.

We found that ϵ = 0.046 allowed for the loosest constraints that produced the maximum number of members in each group but still having velocity and distance dispersions expected for halo substructures. In the following we study with detail the groups found with this value of ϵ. Table 8 indicates the mean properties of the 8 groups (labelled with letters A to H) detected with this value of ϵ, including mean distance and velocity, velocity dispersion, distance dispersion (along the line of sight) and number of members. In addition, we calculated the 3d dispersion, $\sigma 3d$, of each group by obtaining the coordinates of the center of the group from the average of the cartesian coordinates of the members. Then, we estimated the distance separation of each member to the center of the group. The 3d dispersion, which is given in kpc, is the average of those distance separations. Finally the table contains some statistics that help to determine if the

Table 8. Properties of the Groups of RRLS in the Virgo Region detected with $\epsilon = 0.046$

Group	Color/ Symbol	N	$\langle V_{gsr} \rangle$ (km s^{-1})	σV_{gsr} (km s^{-1})	$\langle d \rangle$ (kpc)	σd (kpc)	$\sigma 3d$ (kpc)	P(V_{gsr})	P(d)	P(σd)	P($\sigma 3d$)
A	green/solid squares	9	128	18.9	19.7	1.15	1.57	99.6	98.8	11.3	28.7
B	red/open circles	5	-89	14.7	18.8	0.29	1.42	79.2	90.9	0.6	58.1
C	magenta/solid circles	5	-41	10.6	9.0	0.72	0.95	43.3	37.7	15.4	13.3
D	cyan/solid stars	4	43	11.3	5.4	0.86	0.81	39.4	3.2	40.3	12.1
E	blue/solid triangles	4	95	5.5	11.2	0.75	0.80	77.0	50.4	29.8	11.6
F	black/open stars	4	222	12.8	10.6	1.14	1.45	99.8	46.4	66.0	75.3
G	blue/open triangles	3	57	7.4	16.5	0.33	1.05	46.3	72.4	11.4	52.0
H	pink/open squares	3	173	6.0	12.6	1.01	1.11	96.4	51.9	72.7	59.3

Notes. N is the number of members of the indicated group, P(variable) is the percentile for that group in that particular variable. See text for description.

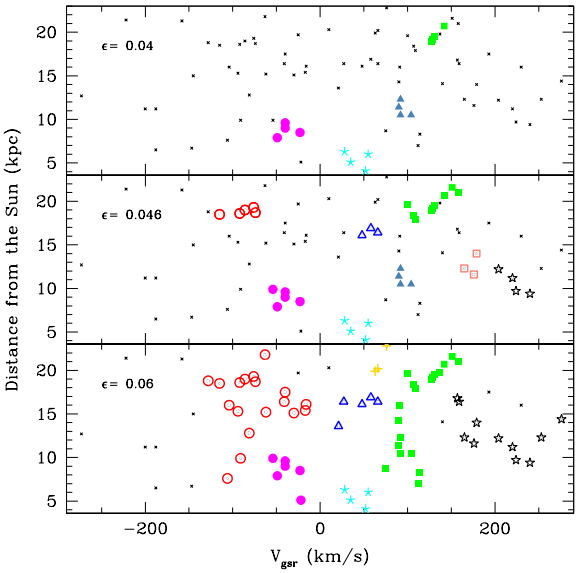

Fig. 9. Distance from the Sun versus radial velocity for all the RRLS in the sample. Groups detected with $\epsilon = 0.04$ (top), 0.046 (middle) and 0.06 (bottom) are shown with different colors/symbols. The properties of the groups shown in the middle panel ($\epsilon = 0.046$) are specified in Table 8.

group is a significant feature of the halo, as we explain in the next section.

4.4. Simulations

A smooth distribution of stars in the sky could produce groups just by random fluctuations. In order to test if our detected groups are special features in the halo or just random fluctuations in a smooth distribution, we performed extensive simulations of random samples of stars. The simulated samples have the following properties:

– Each sample has a random number of stars taken from a Poisson distribution with mean N. The value of N was obtained by integrating the number density profile of RRLS in the halo with the limits in area and depth similar to the observed sample. We obtained that this region of the halo should contain $N_{ab} = 42$ from the halo density profile given in Vivas & Zinn (2006) for type ab stars. By assuming that $N_{ab+c}/N_c = 1.29$ (Layden 1995), we obtain a total number of RRLS (all types) of $N = 54$. This number is significantly lower than the number in our sample of RRLS (79), which is expected because the Vivas & Zinn (2006) profile was measured in regions that do not contain obvious halo substructures, whereas several authors have found evidence of substructures (see above) in the region under study. These substructures are expected to be imprinted on a smooth background of unrelated RRLS. We have used $N = 54$ in our simulations to see if random fluctuations of the background alone can account for any of the groups identified in Table 8.
– A distance was assigned to each star by randomly sampling the density profile of RRLS given in Vivas & Zinn (2006) between 4 and 22 kpc. A random error of 7%, similar to the error of our observations, was added.
– Random coordinates (RA, Dec) were assigned to each star within the limits of the survey area.
– Radial velocities were drawn from a Gaussian distribution with mean 0 km s^{-1} and $\sigma_{los} = 116$ km s^{-1}, which is the value derived by Brown et al. (2010) for stars at $\sim$ 15 kpc from the Sun. A random error of 16 km s^{-1} was added to each simulated star.

This way, we created 10,000 simulated samples and we detected pairs and groups in each one of them using exactly the same procedure as with the RRLS sample. Pairs and groups appeared frequently in the simulated samples. There are enough mock groups in our simulations to test statistically their properties and compare them to our observed groups. In the case of $\epsilon = 0.046$, for example, there are $\sim 36,000$ groups formed in the simulations (an average of ~ 3.6 groups per simulation in 10,000 simulations). Our goal is to see if any of the RRLS groups have properties that are not easily reproduced by the random groups.

Figure 10 shows some of the properties of the groups found in the simulated samples with $\epsilon = 0.046$. Panel (a) shows that most of the mock groups contain only 3 members. The number of mock groups decreases by a factor of ~ 2 for $N_{stars} \geq 4$. In the groups of RRLS we have 2 groups having 3 members each, 3 groups with 4 members, 2 with 5 and 1 with 9 members. It is very rare (< 3%) in our simulations to form a group with 9 or more members. Group A with 9 members is hence, significant.

Figure 10b shows the absolute value of the mean radial velocity of the simulated groups. In this plot the lines indicate the percentiles 75, 90 and 95 in the distribution of velocities of groups with a given N. Most of the groups in the simulated samples have small velocities which agrees with the distribution of velocities given to the random stars. Groups with small N may form with relatively large velocities but with increasing N the largest velocity possible in the groups decreases. The solid points in Figure 10b indicate the velocities of the eight groups of

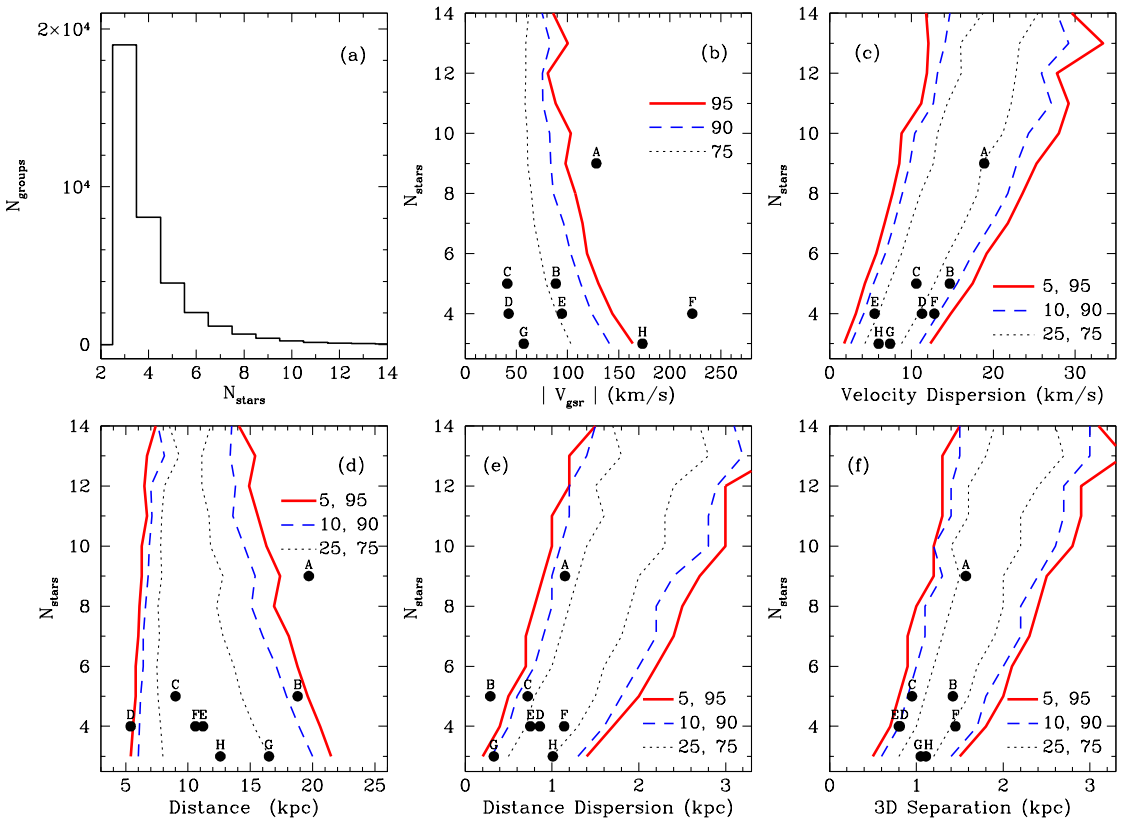

Fig. 10. Properties of the groups found in the simulated samples using $\epsilon = 0.046$. (a) Distribution of the number of stars in the groups. Lines in panels b-f indicate the percentiles 5, 10, 25, 75, 90 and 95 of the distribution of radial velocity (b), velocity dispersion (c), distance (d), distance dispersion (e) and 3D separation (f), for groups having N_{stars} members. For the velocity distribution (b) the x axis shows the absolute value of the velocity and hence, only the percentiles 75, 90 and 95 are indicated. Panels (b) to (f) show the location of groups A to H (Table 8) as solid circles.

RRLS indicated in Table 8. Three of those groups (A, F and H) have velocities which are above the percentile 95 of the distribution. Groups F and H have only 4 and 3 members respectively. Although it is very common to have modelled groups with this low number of stars, it is very rare that they have such a high radial velocity. This fact makes these groups strong candidates to be real features of the halo and not just random fluctuations.

The rest of the panels in Figure 10 shows the distribution of other properties measured in the random groups, namely, velocity dispersion (c), distance (d), distance dispersion (e) and mean separation (3D) from the center of the group (f). For these properties we also show the lines of the percentiles 5, 10 and 25. The mean distance of the groups (Figure 10d) seems to be another parameter that allow us to recognize special features over random fluctuations. At every distance is relatively easy to form groups of small N, but with increasing distance, the decline in the density of RRLS makes it increasingly difficult to form groups of large N. Again, group A, at 19.7 kpc from the Sun, seems special since it is above the 95 percentile of the distance distribution for groups with 9 members. In addition, group B (5 members, 18.8 kpc) is above the 90 percentile for groups of such N.

Group B also stands out because the distance dispersion (Figure 10e) is significantly smaller than any of the random groups. This group has not a particularly small 3D separation, suggesting that the group is more concentrated along the line of sight than across the sky. This may be understood if the stream is crossing almost perpendicularly our line of sight.

4.5. Significant Groups

The analysis of the properties of the simulated groups indicate that some of our groups of RRLS cannot be explained as random fluctuations in the distribution of halo stars. We considered that a group is potentially significant if at least one of their properties is below or above the percentiles 10 and 90 of the distribution of simulated groups for a given N. This way, five of the groups of RRLS have properties that are quite different from groups formed by chance among halo stars. This five groups are thus strong candidates to be real substructures of the halo.

Without a doubt, group A is the most significant feature found in this part of the sky. First it has a very high number of members, which is unusual in the random groups formed in the simulated samples. Furthermore, from the few groups formed with 9 members, none has the combination of mean velocity and distance as group A. This group corresponds to the VSS as first determined by Duffau et al. (2006) and Newberg et al. (2002). The center of the group is found at RA = 186.2°, but it contains stars basically throughout the region explored, from 180° to 195°.

Group B has 5 members and it is also located at a large distance from the Sun, 18.8 kpc. This is above the 90th percentile of the distance distribution for groups with N=5. Group B has another remarkable property and it is that it has a very small dispersion along the line of sight, of only 0.29 kpc, which may be an indication of a thin stream crossing the region perpendicular to the line of sight.

Groups F and H, with 4 and 3 members respectively, have velocities unusually high which make them significant even when having such low number of members. Group F is the same reported already by Vivas et al. (2008).

Finally, group D is unusual because it is formed by the stars closest to the Sun in our sample. It is remarkable that out of the 5 stars with distances closer than 6.5 kpc, 4 of them make a tight group. This group is present even with a low value of ϵ of only 0.035.

The remaining groups, C, E and G may not be significant and thus are not discussed further.

Figure 10 shows that it would be hard to use this method for detecting groups having very low $|V_{\rm gsr}|$ since they are easily formed among field stars. In order to be detected by this method, such groups should have an unusual property such as a very small dispersion in velocity and/or distance.

4.6. Comparison with other Catalogs and Tracers

Several samples of halo stars with both reliable distances and radial velocities are available in the literature. We used those sources to find additional evidence for the kinematical groups described above. We used the new spectroscopic catalog of bright QUEST RRLS, which contains velocity measurements for all the stars in that catalog brighter than $V \sim 16$ (Vivas et al, in preparation). We included in this catalog the velocity measurement of QUEST star #167 made by Casetti-Dinescu et al. (2009), which was associated with the VSS by those authors. We also compared our results with a subset of RRLS in Virgo from the SEKBO and the Catalina catalogs which have spectroscopic information (Prior et al. 2009; Drake et al. 2013). In the case of Catalina, we found 14 stars in common with the QUEST catalog and a comparison of the velocities indicates a systematic offset of 27 km s^{-1} between both catalogs, with the QUEST velocities being larger than Catalina's. For the purposes of this work, we added 27 km s^{-1} to all the velocities in the Catalina catalog. We also made use in this study of the latest version of the catalog of halo red giants in the Spaghetti survey (Starkenburg et al. 2009, and references herein), as well as M giants from Majewski et al. (2004), most of which are probably associated with the Sgr dSph galaxy. There are also several BHB catalogs available, namely, Sirko et al. (2004); Brown et al. (2008) and Brown et al. (2010). All of these catalogs contain stars within or around the region studied in this work, as shown in Figure 11. We explored also the catalog of BHB stars by De Propris et al. (2010) which overlaps our region. However, these BHB stars are located at distances > 28 kpc, and hence they are much farther away than our sample.

In the case of the BHB catalog of Sirko et al. (2004) which is based in SDSS-DR1, we searched for updated radial velocities in SDSS-DR7 in order to overcome any possible systematic error in the radial velocity in this early catalog. In many cases, more than one DR7 spectroscopic measurement was available, and we calculated an error-weighted mean velocity for those stars. On the other hand, the catalog of Brown et al. (2008) is based in 2MASS and, since it is a nearby sample, it may contain thick disk stars as well as halo stars. Following those authors,

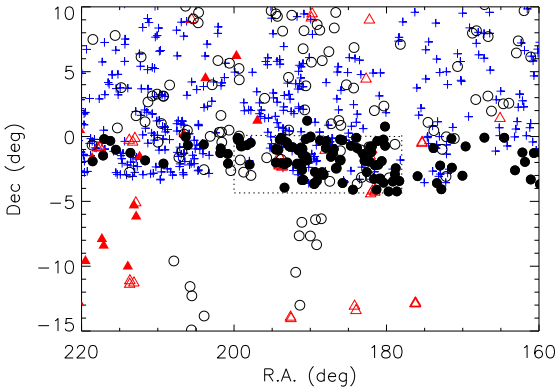

Fig. 11. Distribution in the sky near the Virgo region of halo tracers for which both velocities and distances are available in the literature. Circles represent RRLS (solid circles are stars in the QUEST survey, which includes the ones reported in this work; open circles come from the SEKBO and Catalina surveys), + symbols are BHB stars from Sirko et al. (2004), Brown et al. (2008) and Brown et al. (2010), open and solid triangles are red giants from Starkenburg et al. (2009) and M giants from Majewski et al. (2004), respectively. Notice that the figure shows a region in the sky much larger than the one explored in this work with RRLS, i.e., the dotted rectangle with $178^\circ < {\rm RA} < 200^\circ$, $-4^\circ < {\rm Dec} < 0^\circ$.

we eliminated all stars with $z < 5$ kpc to have a cleaner sample of halo BHBs. We also made sure all radial velocities were in the same frame (the galactic standard of rest) as our sample of RRLS. From Figure 11, there are no BHB data at declinations south of $\sim -3^\circ$, thus the SEKBO, Catalina and Spaghetti samples are specially valuable on those regions.

In order to study which other stars are potentially associated with the groups of RRLS, we determined which RRLS in our significant groups paired with any other star in the additional catalogs, using the same algorithm described above with $\epsilon = 0.05$. In this case, however, we did not weight by the errors since the properties of each catalog are very different from each other. The results are shown in Figure 12. Each row in the figure corresponds to different planes (Dec vs RA, distance vs RA, and distance vs $V_{\rm gsr}$) of the 5 significant groups described in the last section. All these groups have RRLS that pair with several BHB stars and red giants (crosses and triangles respectively). Each one of the groups of RRLS have at least one red giant which is associated with it. Similarly, additional RRLS for each group are provided by either the SEKBO or Catalina catalogs. None of the M giant stars paired with any of our groups. The individual members of each one of these groups are listed in Table 9. The table indicates for each group, the survey from which the member was identified, the type of star used as tracer in that survey (RRLS: RR Lyrae stars, BHB: Blue Horizontal Branch stars, and RG: Red Giant stars), the ID within the survey for the star, its RA and Dec as well as its velocity and heliocentric distance. Finally, the last column gives the corresponding reference. Given the very different properties of the catalogs used, each one having different coverages and completeness, we did not attempt to make simulations to test the significance of those additional members. The additional members suggest possible directions, within the limits of their own surveys, in which follow up observations can focus in the future.

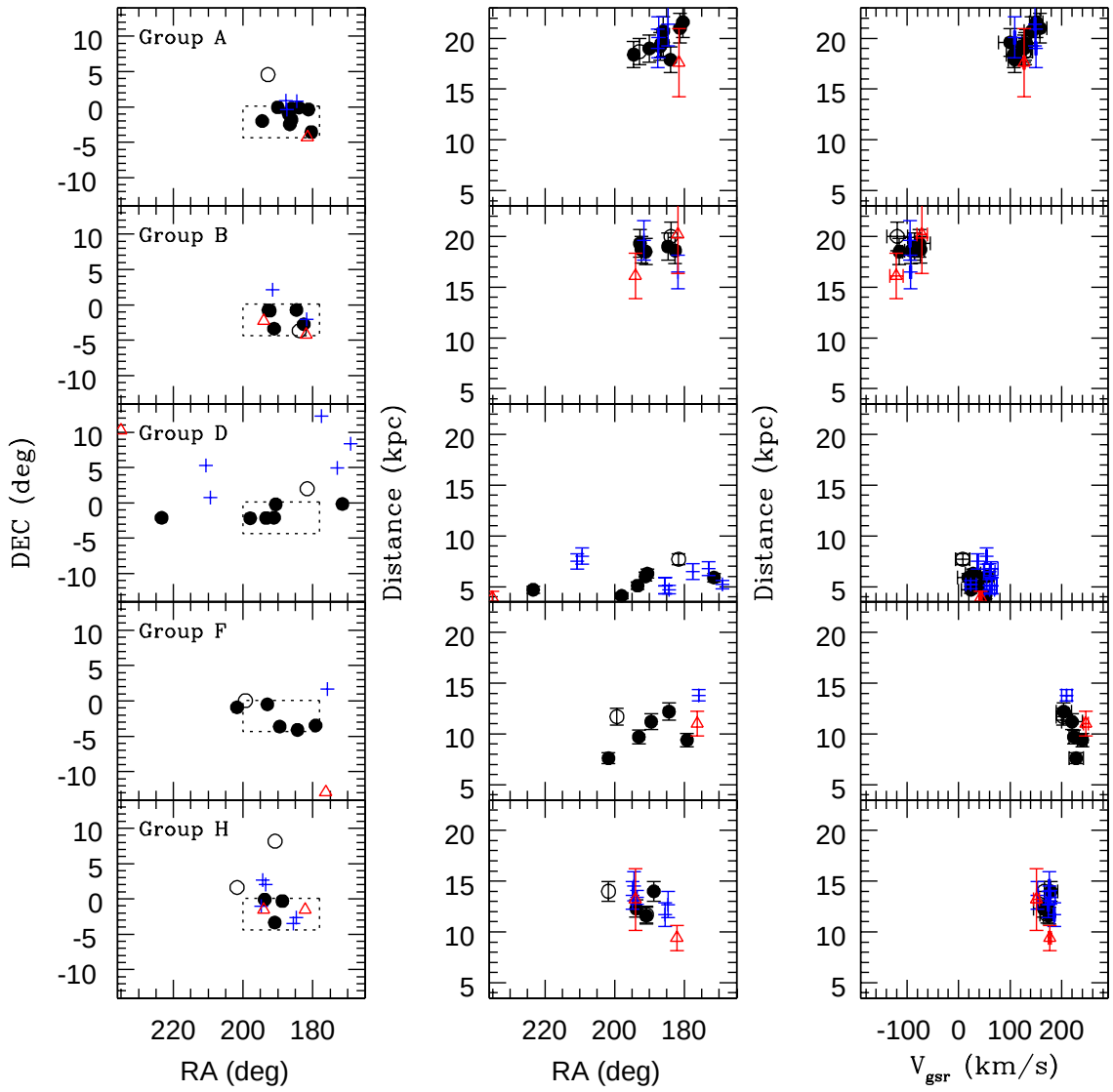

Fig. 12. Distribution in the sky and in phase space of the groups detected in this work. Each row shows different planes for the same group. Symbols are the same as in Figure 11.

The left columns in Figure 12 show the spatial distribution of each group (Dec vs RA). All the groups extend in the sky to some degree in both directions. It is especially noticeable for group D and this is just a consequence of that group being close to the Sun. These plots show us that the five kinematical groups occupy the same region of the sky. The right panels in Figure 12 show the distribution in phase space for every group. It is clear that each group occupies a very different region in this plane making the case that they are distinct structures.

4.7. Properties of the groups

In Table 10 we summarized the main properties of the kinematical groups we have found. The mean properties were calculated using only the RRLS which are members of each group, including the ones from SEKBO, Catalina and from the extended QUEST catalog.

We consider here whether the VSS (group A) may be related with groups F and H. Figure 12 shows there is a sequence in the location of these 3 groups in phase space (rightmost panels in the Figure), with velocity increasing and distance decreasing from group A, to group H, to group F. Table 10 indicates that the properties of the RRLS in these groups are similar and thus, at this point, a relationship among them cannot be discarded. The three groups have similar metallicities, although group A has the largest metallicity dispersion among the three. They also have RRab with similar mean periods, and the type ab dominates over the type c among the RRLS in the three groups.

Carlin et al. (2012) identified turnoff stars with proper motions, in a small region at (RA, Dec) = (178.8°,−0.6°), in order to calculate an orbit for the VSS. It is worth noticing that the properties of those turnoff stars (mean distance=14 kpc, V_{gsr} = 153 km s^{-1}) are more compatible with stars in group H rather than the VSS itself. Ideally, obtaining proper motions in more extended and deeper areas will allow to determine whether the

Table 9. Individual members of kinematical groups

Group	Survey	Tracer	ID	RA	Dec	V_{gsr}	d	Reference
				(deg)	(deg)	(km s^{-1})	(kpc)	
A	QUEST	RRLS	725	180.404037	-3.557914	151	21	This work
A	QUEST	RRLS	177	181.212601	-0.351735	158	21	This work
A	QUEST	RRLS	189	183.965347	-0.098466	109	17	This work
A	QUEST	RRLS	195	186.065384	-1.820641	142	20	This work
A	QUEST	RRLS	196	186.083054	-0.227318	100	19	This work
A	QUEST	RRLS	740	186.586151	-2.446141	131	19	This work
A	QUEST	RRLS	199	186.930542	-0.965226	129	19	This work
A	QUEST	RRLS	210	190.014893	-0.069222	127	19	This work
A	QUEST	RRLS	237	194.513031	-2.009306	107	18	This work
A	CSS	RRLS	J125124.4+043347	192.851690	4.563240	129	18	Drake et al. (2013)
A	SDSS	BHB		187.650010	0.874320	150	19	Sirko et al. (2004)
A	SDSS	BHB		187.396030	-0.409560	109	20	Sirko et al. (2004)
A	SDSS	BHB		184.603940	0.794670	148	21	Sirko et al. (2004)
A	Spaghetti	RG		181.514723	-4.291935	127	17	Starkenburg et al. (2009)

Notes. Only members of group A are shown here. The entire table containing members of all groups is available in the online version of this article. See text for description.

two groups have similar orbits. Curiously, QUEST star #167, which has been associated with the turnoff stars measured by Carlin et al. (2012) does not match either members of group H or any other star in the rest of the groups. After increasing the value of ϵ to 0.06, this star matches 3 members of the VSS (group A) instead.

On the other hand, Newberg et al. (2007) studied a sample of F stars with bluer colors than the ones containing the VSS signature. Among these, one velocity peak of significant relevance is present on the N07 N field at $\gtrsim$ 150 km s^{-1} and at relatively close distances ($<$ 14.5 kpc). Newberg et al. (2007) believed it might be related to the VSS but did not elaborate more on this. We can now connect this feature to our Group H. The presence of this peak on the sample with colors bluer than the VSS turnoff suggest that it is possible that the Group H is actually composed of a different population and as such, it may be a different feature than the VSS. We notice that this group is not present on the N07 S field, suggesting that it is not as extended as the VSS.

Group B is peculiar among the groups because is dominated by type c stars (only 1 out of the 6 RRLS in the group belongs to the type ab class). On the other hand, group D has the largest ratio of BHB/RRLS, although this may be an observational bias given the availability of a large catalog of nearby BHB stars (Brown et al. 2008). Both groups B and D have the shortest mean periods of the RRab stars among all the groups.

4.8. Comparison with Sgr models

Figure 13 (top) shows that the models of Sgr debris by Law & Majewski (2010) indicate that its tidal streams pass close enough to our area of study that we can expect that some of our RRLS belong to this galaxy. Although most of the Sgr stars in the region are located at distances larger than ~40 kpc (bottom panel in Figure 13), there are some particles at closer distances, within the range studied in this work. However, the nearby debris does not seem to be related with any of the kinematical groups found in this work, shown as coloured symbols in Figure 13. None of our groups have either the velocity or the distance for the expected Sgr debris in the region.

There is a small number of nearby Sgr debris stars in this part of the sky (distance $\lesssim$ 11 kpc, -160 $\lesssim$ V_{gsr} (km s^{-1}) $\lesssim$ -90). According to Law & Majewski (2010) this part of the stream is

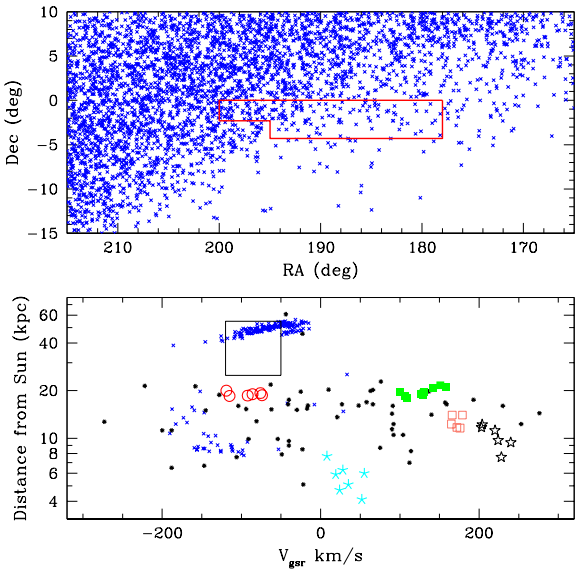

Fig. 13. Top: Distribution in the sky around Virgo of the Sgr debris in the models of Law & Majewski (2010). The polygon indicates the region studied in this work. Bottom: Velocity and distance of model particles (crosses) and RRLS (asterisks) within the box indicated above. Stars in each one of the 5 kinematical groups detected here are shown with their corresponding symbol (Table 8). The two RRLS at distances > 40 kpc were taken from Vivas et al. (2005). Rectangle indicates the approximate location of another kinematical group found by Brink et al. (2010) and Casey et al. (2012).

made of stars that were mostly stripped from Sgr between 3.2 to 5.0 Gyrs ago. The small number of model particles translates in an even smaller number of RRLS predicted to exist in that nearby stream. Zinn et al. (2014) estimated that for every particle in the model of Law & Majewski (2010) there are $\sim$ 0.23 RRLS. Thus, with 24 particles in that nearby stream, there should be $\sim$ 5 Sgr RRLS in the region. While there are 3 RRLS which have similar distance and velocity than the stream (see Figure 13), we also expect, from the simulations described in Section 4.4, 4 ± 2 halo RRLS in the same region of the phase

Table 10. Properties of the groups

Group	RA	N_{RR}	N_{BHB}	N_{BHB}/N_{RR}	RR_c/RR_{ab}	P_{ab}	[Fe/H]	σ[Fe/H]	$\langle V_{gsr} \rangle$	σV_{gsr}	$\langle d \rangle$
	(deg)					(d)			(km s^{-1})	(km s^{-1})	kpc
A	186.863	10	3	0.3	0.11	0.56	-1.78	0.37	128	18	19.6
B	187.879	6	2	0.3	5.00	0.52	-1.69	0.18	-94	18	19.0
D	192.792	7	8	1.1	0.40	0.55	-1.64	0.09	32	16	5.7
F	191.194	6	2	0.3	0.00	0.59	-1.62	0.19	220	13	10.3
H	193.187	5	1	0.2	0.00	0.57	-1.72	0.21	172	6	12.7

space. Thus, there is not a clear excess of RRLS that can be readily associated with this stream from an old wrap. A similar conclusion on the lack of strong evidence for a stream stripped between 3.2 to 5 Gyrs ago was made by Zinn et al. (2014) based on the spatial distribution of a larger sample of RR Lyrae stars.

The bottom panel in Figure 13 also shows the regions where other kinematical signatures have been found by other groups. Brink et al. (2010) and Casey et al. (2012) studied the velocity distribution of main sequence stars and red giants in the region, respectively (see Figure 3). Although Brink et al. (2010) and Casey et al. (2012) state somewhat different ranges for their velocity features, they are consistent with a mean velocity of ~ -80 km s^{-1} . This velocity is sufficiently close to mean velocity of Group B that they may be related. However, the majority of the stars in both the Brink et al. (2010) and the Casey et al. (2012) samples are probably more distant that 20 kpc, and they may instead be related to the Sgr stream, which lies at $\sim$ 50 kpc, or with the substructure recently identified by Jerjen et al. (2013)) at $\sim$ 23 kpc, whose velocity has not yet been measured.

5. CONCLUSIONS

We present the first complete spectroscopic study of all RRLS in the QUEST survey in the direction of the VSS. For this work we have gathered 82 targets combining two previous works by the collaboration (Duffau et al. 2006; Vivas et al. 2008), and reporting on 36 RRLS newly observed stars. The sample covers heliocentric distances between 4-23 kpc, $\sim$ 90 square degrees, and RA between 178°-200°. This homogeneous sample enables us to disentangle in phase space several substructures lying along the same line of sight. This is possible because RRLS are excellent standard candles and allow the determination of precise distances.

A summary of all kinematic groups found in the Virgo region is displayed in Table 11. In this table, each check mark ($\surd$) under a study reference represents a detection of the corresponding group. The corresponding references to each study are: N07 (Newberg et al. 2007), B10 (Brink et al. 2010), C12 (Casey et al. 2012), S09 (Starkenburg et al. 2009) and P09 (Prior et al. 2009). The first column contains, in addition to the 5 groups of RRLS detected here, two groups predicted to lie in this region by the models of the disruption of Sgr ("Sgr far" refers to stars located at distances $>$ 40 kpc, while "Sgr near" correspond to stars between $\sim$ 8 and 18 kpc, as shown by the debris (asterisks) in Figure 13). An asterisk in Table 11 indicates a weak detection of the corresponding group.

The VSS, which is now reconciled with feature S297+63-20.5 (Newberg et al. 2007), is the most significant feature in our sample. It spans at least between 17.9-21.6 kpc along the line of sight and has a mean radial velocity of 128 km s^{-1}, as deduced from its RRLS components. A possible relationship of the VSS with two other groups (Groups F and H) cannot be discarded at this point. The three groups form a sequence in phase space with the VSS and group F at the two ends of the sequence with group H intermediate in both velocity and distance (see Figure 12 and Figure 13).

Another significant group, composed mostly of type c stars, was found at a similar distance than the VSS, 19 kpc, but with a velocity of -94 km s^{-1}. Similar velocity signatures have been found in the region by (Brink et al. 2010) and Newberg et al. (2007), although the latter found it among the brightest stars in their sample, hence, presumably corresponding to a group at a shorter distance than our detection. Finally, a nearby group at only 6 kpc was also detected with a mean velocity of $V_{gsr} = 32$ km s^{-1}. The properties of this group are harder to isolate due to its much larger angular extension in the sky and its velocity being close to the expected mean velocity of halo stars.

Using the models of Law & Majewski (2010), we find that while the Sgr stream debris are not expected to be dense in this region at distances closer than 40 kpc, some debris is expected to be found in the VSS area. Several of our RRLS lie within the expected distance and velocity of those predictions. However, none of the kinematic groups we found in this work seem to be related with Sgr debris. For the distances involved in this study the dominant feature is the VSS. This was not the case in the works of Brink et al. (2010) and Casey et al. (2012). Their exploration included targets presumably at much larger distances. In those cases, the dominant feature seems to be the Sgr leading stream or another new sub-structure in the region as suggested by Jerjen et al. (2013).

The numerous kinematic features found in our sample of RRLS qualitatively agree with the expectations of halo substructures in cosmological models of galaxy formation. Our results suggest that several streams, rather than a single accretion event, are responsible for the excess of stars found in the Virgo region.

The true shape and extension of all the streams detected in this work will require accurate distances and velocities of targets in a more extended region than the one considered here. The possibility of clarifying which of the different substructures are related to each other and which are not, might require additional information. One possibility is the chemical tagging of their stars, which is one direction we are currently pursuing.

Acknowledgements. We thank the anonymous referee for useful suggestions and comments. We thank Amina Helmi for kindly providing us the data of the red giants found in the Spaghetti survey. We thank Dana Casetti-Dinescu for kindly providing her orbit for RRL 167. S.D. acknowledges the support from both ARI and CIDA during her visit to CIDA, Venezuela in November 2010 to work in this project, and to Yale/U. de Chile through the joint PhD program (MECESUP UCH0118, Fundacion Andes C13798, Fondap 15010003 and CONICYT 24070078. S.D. also acknowledges support from Sonderforschungsbereich SFB 881 The Milky Way System (subprojects A2, A3 and A4) of the German Research Foundation (DFG). R.Z. acknowledges support from National Science Foundation grants AST 05-07364 and AST 11-08948. M.T.R and R.M. received partial support from CATA (PB06) CONICYT. A.K.V. thanks the hospitality of the Department of Astronomy at University of Michigan during her sabbatical leave in which part of this work was made.

This research was based on data obtained at KPNO (Kitt Peak National Observatory, National Optical Astronomy Observatory, which is operated by the

Table 11. Kinematic Detections in the Virgo Region

Group	This work RRLS	N07 F-TO	B10 F-TO	C12 K-giants	S09 K-giants	P09 RRLS
Group A (VSS)	√	√	√	√		√
Group B	√	*	√			
Group D	√					
Group F	√		√	√		
Group H	√	√			√	
Sgr far			√	√		
Sgr near		√	*		√	√

Association of Universities for Research in Astronomy (AURA) under cooperative agreement with the National Science Foundation), WIYN (The WIYN Observatory is a joint facility of the University of WIsconsin-Madison, Indiana University, Yale University, and the National Optical Astronomy Observatory), CTIO (Cerro Tololo Inter-American Observatory, National Optical Astronomy Observatory, which is operated by the Association of Universities for Reseach in Astronomy, under contract with the National Science Foundation), telescopes at the European Southern Observatory La Silla, Magellan's Clay telescope at LCO (operated by a consortium consisting of the Carnegie Institution of Washington, Harvard University, MIT, the University of Michigan, and the University of Arizona) and instruments operated by the SMARTS Consortium. We thank the staff at all of these observatories for their help during the time the observations were conducted.

References

Baltay, C., Snyder, J. A., Andrews, P., et al. 2002, PASP, 114, 780
Bell, E. F., Zucker, D. B., Belokurov, V., et al. 2008, ApJ, 680, 295
Belokurov, V., Zucker, D. B., Evans, N. W., et al. 2006, ApJ, 642, L137
Bonaca, A., Jurić, M., Ivezić, Ž., et al. 2012, AJ, 143, 105
Brink, T. G., Mateo, M., & Martínez-Delgado, D. 2010, AJ, 140, 1337
Brown, W. R., Beers, T. C., Wilhelm, R., et al. 2008, AJ, 135, 564
Brown, W. R., Geller, M. J., Kenyon, S. J., & Diaferio, A. 2010, AJ, 139, 59
Bullock, J. S. & Johnston, K. V. 2005, ApJ, 635, 931
Carlin, J. L., Yam, W., Casetti-Dinescu, D. I., et al. 2012, ApJ, 753, 145
Casetti-Dinescu, D. I., Girard, T. M., Majewski, S. R., et al. 2009, ApJ, 701, L29
Casey, A. R., Keller, S. C., & Da Costa, G. 2012, AJ, 143, 88
Clewley, L. & Kinman, T. D. 2006, MNRAS, 371, L11
Cooper, A. P., Cole, S., Frenk, C. S., et al. 2010, MNRAS, 406, 744
De Propris, R., Harrison, C. D., & Mares, P. J. 2010, ApJ, 719, 1582
Demarque, P., Zinn, R., Lee, Y.-W., & Yi, S. 2000, AJ, 119, 1398
Drake, A. J., Catelan, M., Djorgovski, S. G., et al. 2013, ApJ, 763, 32
Duffau, S., Zinn, R., Vivas, A. K., et al. 2006, ApJ, 636, L97
Helmi, A., Cooper, A. P., White, S. D. M., et al. 2011, ApJ, 733, L7
Ivezić, Ž., Goldston, J., Finlator, K., et al. 2000, AJ, 120, 963
Jerjen, H., Da Costa, G. S., Willman, B., et al. 2013, ApJ, 769, 14
Jurić, M., Ivezić, Ž., Brooks, A., et al. 2008, ApJ, 673, 864
Keller, S. C. 2010, PASA, 27, 45
Keller, S. C., da Costa, G. S., & Prior, S. L. 2009, MNRAS, 394, 1045
Keller, S. C., Murphy, S., Prior, S., Da Costa, G., & Schmidt, B. 2008, ApJ, 678, 851
Law, D. R. & Majewski, S. R. 2010, ApJ, 714, 229
Layden, A. C. 1994, AJ, 108, 1016
Layden, A. C. 1995, AJ, 110, 2288
Layden, A. C. 1998, AJ, 115, 193
Majewski, S. R., Kunkel, W. E., Law, D. R., et al. 2004, AJ, 128, 245
Majewski, S. R., Skrutskie, M. F., Weinberg, M. D., & Ostheimer, J. C. 2003, ApJ, 599, 1082
Martínez-Delgado, D., Peñarrubia, J., Jurić, M., Alfaro, E. J., & Ivezić, Z. 2007, ApJ, 660, 1264
Moultaka, J., Ilovaisky, S. A., Prugniel, P., & Soubiran, C. 2004, PASP, 116, 693
Newberg, H. J., Yanny, B., Cole, N., et al. 2007, ApJ, 668, 221
Newberg, H. J., Yanny, B., Rockosi, C., et al. 2002, ApJ, 569, 245
Preston, G. W. & Sneden, C. 2000, AJ, 120, 1014
Prior, S. L., Da Costa, G. S., Keller, S. C., & Murphy, S. J. 2009, ApJ, 691, 306
Sesar, B., Ivezić, Ž., Lupton, R. H., et al. 2007, AJ, 134, 2236
Sirko, E., Goodman, J., Knapp, G. R., et al. 2004, AJ, 127, 899
Starkenburg, E., Helmi, A., Morrison, H. L., et al. 2009, ApJ, 698, 567
Vivas, A. K. 2002, PhD thesis, AA(YALE UNIVERSITY)
Vivas, A. K., Jaffé, Y. L., Zinn, R., et al. 2008, AJ, 136, 1645
Vivas, A. K. & Zinn, R. 2006, AJ, 132, 714
Vivas, A. K., Zinn, R., Abad, C., et al. 2004, AJ, 127, 1158
Vivas, A. K., Zinn, R., Andrews, P., et al. 2001, ApJ, 554, L33
Vivas, A. K., Zinn, R., & Gallart, C. 2005, AJ, 129, 189
Walsh, S. M., Willman, B., & Jerjen, H. 2009, AJ, 137, 450
Wu, C., Qiu, Y. L., Deng, J. S., Hu, J. Y., & Zhao, Y. H. 2005, AJ, 130, 1640
Xue, X.-X., Rix, H.-W., Yanny, B., et al. 2011, ApJ, 738, 79
Zinn, R., Horowitz, B., Vivas, A. K., et al. 2014, ApJ, 781, 22